Received Date : 19-Aug-2016

Revised Date : 12-Dec-2016

Accepted Date : 14-Dec-2016

Article type : Original Article

TaADF4, an actin-depolymerizing factor from wheat, is required for resistance to the stripe rust pathogen *Puccinia striiformis* f. sp. *tritici*

Bing Zhang[1,2], Yuan Hua[1], Juan Wang[1], Yan Huo[1], Masaki Shimono[2], Brad Day[2,*], and Qing Ma[1,*]

[1]State Key Laboratory of Crop Stress Biology for Arid Areas, Northwest A&F University, Yangling, Shaanxi 712100, China. [2]Michigan State University, Department of Plant, Soil and Microbial Sciences, East Lansing, Michigan 48824, USA.

*Co-corresponding Authors

Brad Day

Michigan State University

Department of Plant, Soil and Microbial Sciences

1066 Bogue Street, A286

East Lansing, Michigan 48824, USA

E: bday@msu.edu

P: +1-517-353-7991

This article has been accepted for publication and undergone full peer review but has not been through the copyediting, typesetting, pagination and proofreading process, which may lead to differences between this version and the Version of Record. Please cite this article as doi: 10.1111/tpj.13459

Qing Ma

State Key Laboratory of Crop Stress Biology for Arid Areas

Northwest A&F University

Yangling, Shaanxi 712100, China

E: maqing@nwsuaf.edu.cn

P: +86-029-87082401

Running Title: ADF4 is required for resistance to stripe rust

Keywords: *Puccinia striiformis* f. sp. *tritici*, wheat, actin, ADF4, resistance, cytoskeleton, *Triticum aestivum*

SUMMARY

Actin filament assembly in plants is a dynamic process, requiring the activity of more than 75 actin-binding proteins. Central to the regulation of filament assembly and stability is the activity of a conserved family of actin-depolymerizing factors (ADFs), whose primarily function is to regulate actin filament severing and depolymerization. In recent years, the activity of ADF proteins has been linked to a variety of cellular processes, including those associated with response to stress. Herein, a wheat *ADF* gene, *TaADF4,* was identified and characterized. *TaADF4* encodes a 139-amino acid protein containing five F-actin binding sites and two G-actin binding sites, and interacts with wheat (*Triticum aestivum*) Actin1 (*i.e., Ta*ACT1), *in planta*. Following treatment of wheat, separately, with jasmonic acid, abscisic acid, or with the avirulent race, CYR23, of the stripe rust pathogen *Puccinia striiformis* f. sp. *tritici*, we observed a rapid induction in *TaADF4* mRNA accumulation. Interestingly, *TaADF4* mRNA accumulation was diminished in response to inoculation with a virulent race, CYR31. Silencing of *TaADF4* resulted in enhanced susceptibility to CYR23, demonstrating a role for *TaADF4* in defense signaling. Using a pharmacological-based approach, coupled with an analysis of host response to pathogen infection, we observed that treatment of plants with the actin modifying agent latrunculin B enhanced resistance to CYR23, including an increased production of reactive oxygen species and an enhancement of localized hypersensitive cell death. Taken together, these data support the hypothesis that *Ta*ADF4 positively modulates plant immunity in wheat *via* the modulation of actin cytoskeletal organization.

INTRODUCTION

Wheat (*Triticum aestivum*) stripe rust (*Puccinia striiformis* f. sp. *tritici*; hereafter *Pst*) is the most devastating pathogen of all the wheat rusts, impacting global production with an estimated $979M in annual losses (Beddow *et al*., 2015; Akin *et al.*, 2016). Indeed, In recent years, the spread of the pathogen, coupled with an increase in the total planting area of wheat, has resulted in *Pst* becoming the most threatening of the cereal pathogens (Milus *et al.*, 2009; Hovmøller *et al.*, 2010; Jin *et al.*, 2010; Zhao *et al.*, 2011). Coupled with the emergence of new pathotypes, an alarming number of known rust resistance genes in wheat are no longer effective, thus rendering previously resistant cultivars susceptible (Chen, 2005; Sharma-Poudyal *et al.,* 2013). While several reports have provided insight into the infection and host resistance processes activated during infection (Chen *et al*., 2002; Kang *et al*., 2002; Wang *et al*., 2007; Chen *et al.*, 2014), a full understanding of the mechanisms underpinning resistance to *Pst* remains largely undefined.

In plants, the mechanisms underpinning resistance to pathogen infection, including the basis of host range and virulence, is driven by complex, co-evolved determinants from host and pathogen. In the broadest sense, immune signaling is mediated by at least two, co-regulated, and well-characterized signaling cascades. The first, pathogen associated molecular pattern (PAMP) triggered immunity (PTI), is activated following the perception of conserved features of the pathogen (e.g., flagellin, chitin) by extracellular pattern recognition reception within the plant. The outcome of this recognition is the activation of rapid, broad, host responses that in most instances abrogate pathogen invasion and proliferation. As a second layer of the host immune system, plants utilize a highly-specific and robust PTI-like response termed effector-triggered immunity (ETI), which is mediated by the recognition of secreted pathogen molecules, known as effectors, by host resistance (R) proteins. In this cascade, upon recognition of the effectors by the R-proteins, localized cell death (i.e., the hypersensitive response (HR)) is observed, which ultimately manifests as resistance (Chisholm *et al*., 2006; Jones and Dangl, 2006). At a molecular and cellular level, the function of the effector-R-protein interaction is hypothesized to activate a robust immune signaling cascade that enables plants to restrict pathogen access to nutrients, thereby halting pathogen growth. While often described as separate pathways, recent research suggests that PTI and ETI share numerous convergent signaling processes.

The actin cytoskeleton plays a key role in the activation of plant immune signaling, including in pathogen perception and the amplification of numerous downstream signaling processes required for host resistance to pathogen infection (Schmidt and Panstruga, 2007; Day *et al*., 2011). For example, work in this area has demonstrated that the plant actin cytoskeleton is an essential

component of PTI (Hardham *et al*., 2007; Henty-Ridilla *et al*., 2013), ETI (Tian *et al*., 2009; Porter *et al*., 2012), is a target of pathogen effectors (Kang *et al*., 2014; Shimono *et al*., 2016b), and supports numerous cellular processes required for pathogen resistance (Yun *et al*., 2003; Fu *et al*., 2014; Tang *et al*., 2015; Shimono *et al*., 2016a). To define the role of the plant actin cytoskeleton during pathogen infection, much of the early work in this area focused on the spatial and temporal changes in actin cytoskeletal organization during the elicitation of the HR. For example, numerous studies shown that actin filaments form radial bundles concentrating at the side of infection, providing an architectural and structural basis for what is defined as penetration resistance (Kobayashi *et al*., 1994; Kobayashi *et al*., 1997; Skalamera and Heath, 1998; Yun *et al*., 2003; Shimada *et al*., 2006; Miklis *et al*., 2007; Hardham, Jones and Takemoto, 2007). The activity of the actin cytoskeleton has also been linked to immunity in barley (*Hordeum vulgare*), through observation that the non-pathogen *Erysiphe pisi* was able to penetrate and form haustoria in barley coleoptile cells when treated with actin modifying agents (Kobayashi *et al*., 1997). Overall, these studies provide compelling evidence that modifications to the host actin cytoskeleton promote both resistance and susceptibility, establishing the plant actin cytoskeleton as a critical component of the immune signaling network.

One of the key regulators of actin cytoskeletal organization and function is a family of highly conserved proteins known as actin depolymerizing factors (ADFs), a family of small proteins (15-22 kDa) found in all eukaryotes that are responsible for actin filament severing and depolymerization. In recent years, ADF proteins from a variety of plants have been demonstrated to play key roles in the modulation of host immunity following pathogen perception, including in response to bacterial (Tian *et al*., 2009; Porter *et al*., 2012), and fungal (Fu *et al*., 2014; Tang *et al*., 2015; Inada *et al*., 2016) infection. In the current study, we used a combination of genetic-, cellular-, and pharmacological-based approaches to define the function of *Ta*ADF4 during pathogen infection. In short, we demonstrate that *Ta*ADF4 expression is necessary and required for resistance signaling in response to infection with the *Pst* race CYR23. In addition to its role in resistance, an evaluation of its expression suggests that *Ta*ADF4 is also required for broader host responses to stress perception and signaling, including in response to changes in temperature and hormone signaling. In total, the current work described herein provides evidence supporting the link between the dynamic reorganization of the plant actin cytoskeleton and the activation of immune signaling following pathogen infection.

RESULTS

Identification and sequence analysis of wheat *ADF4*

Using the sequence of an ADF gene from barley as an *in silico* probe, a 687-nucleotide cDNA clone was identified and cloned from the wheat cultivar Suwon 11. The isolated wheat ADF gene contained a deduced open reading frame of 420 bp, encoding a putative protein of 140 amino acids. As shown in Figure 1a, *in silico*-based sequence analysis revealed that *Ta*ADF4 is most similar to *Secale cereale* × *Triticum* ADF4-1 and *Secale cereale* × *Triticum* ADF4-2, with a maximal identity of 99%. As it possesses 84% amino acid sequence identity to *Arabidopsis thaliana At*ADF4 (Tian *et al*., 2009), it was named *Ta*ADF4 (GenBank accession number KF246580). The translated cDNA of *TaADF4* yields a protein with a molecular weight of approximately 16 kDa, with a theoretical isoelectric point (i.e., pI) of 5.59.

As shown in Figure 1b, *Ta*ADF4 falls within a clade of conserved proteins within which *Ta*ADF4, *Sc* × *Td*ADF4-1, *Ta*ADF11, and several *Arabidopsis* ADFs including *At*ADF4 are tightly clustered, while *Os*ADF1, *Os*ADF7, and *Ta*ADF7 were similarly, yet distinguishably, clustered. We posit that the close evolutionary relationship between *Ta*ADF4, *Ta*ADF7, *At*ADF4, and *Os*ADF1 suggests the potential for similar functions in their respective hosts, including conserved roles in biotic and abiotic interactions. SMART analysis (Schultz *et al*., 1998) revealed that *Ta*ADF4 possesses a conserved ADF domain (amino acids 6-138), five F-actin binding sites (amino acids 82, 84, 98, 125, and 128), and two G-actin binding sites (amino acids 6 and 7). Further *in silico* analyses revealed that *Ta*ADF4 contains six additional motifs, including three predicted protein kinase C phosphorylation sites (amino acids 26-28, 94-96, and 105-107), two casein kinase II phosphorylation sites (amino acids 52-55 and 105-108), and one N-myristoylation site (amino acids 7-12) (Figure 1c). Lastly, homology modeling of the *Arabidopsis* and wheat ADF4 proteins showed that the predicted tertiary structures are highly similar (Figure 1d).

*Ta*ADFs differentially, and specifically, interact with ACTIN *in vivo*

One of the outstanding questions with respect to plant cytoskeletal function is that of the functional relationship(s) between the large numbers of ADF proteins versus the similarly large number of actin isoforms (Šlajcherová *et al*., 2012). For example, 8 ADFs and 2 actin (ACT) isoforms have been isolated from wheat, while *Arabidopsis* contains 11 ADF and 8 ACT isoforms (Huang *et al*., 1997; Kandasamy *et al*., 2001; Ruzicka *et al*., 2007). Conversely, humans possess 3 ADF isoforms and 3 ACT isoforms (Dominguez and Holmes, 2011).

As an initial step towards defining the interaction network of the wheat and *Arabidopsis* ADF4 proteins, we conducted a yeast-two-hybrid (Y2H) screen using *Ta*ADF4 and *At*ADF4. As shown in Table S1, we identified approximately 18 and 25 putative *Arabidopsis* protein interactions using *Ta*ADF4 and *At*ADF4 as baits, respectively. As predicted, and in support of our working hypothesis derived from phylogenetic and *in silico* functional analyses (Figure 1), we identified several shared interactions between *Ta*ADF4 and *At*ADF4, suggesting that ADF isoforms likely possess similar functions based on evolutionarily relatedness. Of the shared interactions, we chose to focus on the interaction with ADF4 and the actin isoform ACT7, which has previously been shown to respond to hormone application, light, and wounding (McDowell *et al*., 1996; Kandasamy *et al*., 2001; Gilliland *et al*., 2003).

To confirm that the ADF-ACT interaction identified by Y2H (Figure 2a), we next performed co-immunprecipitation (co-IP) assays of T7-epitope-tagged *At*ADF4 and *Ta*ADF4, and Myc-epitope-tagged *At*ACT7 and *Ta*ACT1 using *Agrobacterium*-mediated transient expression in *Nicotiana benthamiana*. As shown in Figure 2b, we identified interactions between *At*ADF4-*At*ACT7 and *Ta*ADF4-*Ta*ACT1 *in planta*, with additional reciprocal interaction assays between *At*ADF4 and *Ta*ACT1, *Ta*ADF4, and *At*ACT7, further supporting our observations (Figure S1).

Next, to define the interaction specificity between wheat ADFs and ACT1, we next tested the interactions between *Ta*ADF3, *Ta*ADF4, *Ta*ADF5, *Ta*ADF6, *Ta*ADF7, *Ta*ADF8 and *Ta*ACT1, using a series of directed protein-protein Y2H interaction screens. As shown in Figure 2c, we identified positive interactions between *Ta*ADF3, *Ta*ADF4, *Ta*ADF5, *Ta*ADF6, *Ta*ADF7 and *Ta*ACT1, but did not observe an interaction between *Ta*ADF8 and *Ta*ACT1. As a possible explanation for the observed interaction specificity, and lack thereof with respect to *Ta*ADF8 and *Ta*ACT1, using homology modeling of the predicted three-dimensional structures of the ADF proteins, we found that *Ta*ADF3, *Ta*ADF4, *Ta*ADF5, *Ta*ADF6, and *Ta*ADF7 almost completely overlapped with each other (Figure 2d, left). The predicted model of *Ta*ADF8 did not possess a substantial overlap with any of the other ADFs tested, with differences in the numbers of alpha helices and beta sheets (Figure 2d, right).

Finally, in addition to identifying the interaction between TaADF4 and actin using Y2H and co-immunoprecipitation, above, we further investigated the activity of TaADF4 in binding to actin filaments *in vivo*, as well as to determine the effect(s) of the F-actin assembly inhibitor LatB on the organization of actin filaments using confocal microscopy analyses. As shown in Figure 3a, following co-expression of *Ta*ADF4-RFP and *Ta*ACT1-GFP by Agrobacterium infiltration in *N. benthamiana*, we observed that *Ta*ADF4-RFP co-localized to actin filaments, in agreement with our Y2H and co-immunoprecipitation data. Furthermore, we observed significant depolymerization in both *Ta*ADF4-RFP and *Ta*ACT1-GFP labeled filaments at 6h after LatB treatment (Figure 3b), establishing that these two proteins are in fact associated with F-actin filaments. Negative control infiltrations, consisting of *Ta*ADF4 co-infiltrated with GFP alone and *Ta*ACT1 co-infiltrated with RFP, are shown in Figure S2.

***TaADF4* mRNA accumulation is induced following abiotic and biotic stress perception**

As a first step in defining the role of *Ta*ADF4 in broader stress signaling responses in wheat, we first investigated the expression patterns of *TaADF4* following abiotic and biotic stress perception. As shown in Figure 4a, we defined the spatial expression pattern of *TaADF4* from a variety of samples, including seeds, roots, the root-stem junctions, stems and leaves. As shown, *TaADF4* mRNA was detected in each of the five sample types tested, with the highest level of expression found in RNA samples from the root-stem junction and leaves.

To evaluate the expression dynamics of *TaADF4* following abiotic and biotic stress perception, we next assessed the effect of phytohormones and environmental stressors on *TaADF4* mRNA accumulation using qRT-PCR. First, and as presented in Figure 4b, we monitored *TaADF4* mRNA accumulation in wheat following exogenous application of the 4 primary stress-associated hormones: ethylene (ET), methyl jasmonate (Me-JA), abscisic acid (ABA), and salicylic acid (SA). As shown, we did not observe a significant change in the expression of *TaADF4* following ET treatment over a 24 h time-course of sampling. This was not surprising, as previous work has shown that ET induces changes in microtubule organization (Takahashi *et al.*,; 2003 Plett *et al.,* 2009) and to date, no induced changes in the actin cytoskeleton have been reported in response to ET perception. Conversely, we did observe a significant increase at 24 hpt in the accumulation of *TaADF4* mRNA following Me-JA treatment, in agreement with previous work from our group that identified a relationship between actin, pathogen infection, and the expression of JA-specific markers (Tian *et al*., 2009). Similarly, we observed a marked increase in *TaADF4* mRNA accumulation at 2 hpt

following ABA treatment, again in agreement with previous work demonstrating that ABA is associated with the modulation of actin dyanmics *via* a direct or indirect function of ADF phosphorylation status (Chen *et al*., 2006). Finally, we observed on a modest increase in the expression of *TaADF4* following SA application, with an approximate 1.5-fold increase from 30 minutes to 12 hpt.

Previous work has shown that the actin cytoskeleton responds to abiotic perception (Ouellet *et al*., 2001; Huang *et al*., 2012). To determine if mRNA accumulation is impacted by abiotic stress, we next analyzed the expression of *TaADF4* following exposure of plants to 4 environmental stressors: drought, high temperature, low temperature, and salinity. As shown in Figure 4c, we did not observe a significant change in the accumulation of *TaADF4* mRNA following PEG6000 treatment over the 24 h sampling period. However, we observed an approximate 1.5-fold, rapid, increase in the expression of *TaADF4* following exposure to high temperature (37°C) at 1 hpt, followed by a return to basal expression by 3 hpt. Interestingly, a second increase was observed at 12 hpt, again with a return to basal expression levels at 24 hpt. We posit that this bimodal expression of *TaADF4* may be illustrative of the rapid cycling of actin assembly and disassembly, potentially as an initial stress-induced response, followed by a return to homeostatic cycling – a process that has previously been shown to be required for cellular transport within the cytoplasm at higher temperatures (Lappalainen and Drubin, 1997; Stamnes, 2002). Conversely, following low-temperature and high salt treatment, we observed a complete absence in the mRNA accumulation of *TaADF4*, indicating that these 2 stressors have a significant impact on ADF expression. This observation is in agreement with previous studies that have shown an impact on the physical organization of actin following low temperature and salt stresses (Ouellet *et al*., 2001; Yan *et al*., 2005).

Lastly, we monitored the expression of *TaADF4* following infection of wheat seedlings with a virulent and avirulent race of *Pst.* As shown in Figure 4d, we observed a general increase in *TaADF4* mRNA accumulation during the incompatible interaction (i.e., *Pst* CYR23), with an approximate 2-fold induction at 6 hpi, and a >4-fold increase in expression at 18-72 hpi. Conversely, we observed a decrease in *TaADF4* mRNA accumulation in the compatible interaction (i.e., *Pst* CYR31) compared with untreated seedlings. The maximal differences in mRNA accumulation between incompatible and compatible interactions were at 18 hpi (ca. 13-fold), 48 hpi (ca. 8-fold), and 72 hpi (ca. 4-fold).

TaADF4 is required for resistance to _Puccinia striiformis_ f. sp. _tritici_

To determine the role of *TaADF4* during host infection by *Pst*, we used a Barley stripe mosaic virus-induced gene silencing (BSMV-VIGS)-based approach (Holzberg *et al*., 2002; Scofield *et al*., 2005; Bennypaul *et al*., 2012) to knockdown *TaADF4* expression in the wheat cultivar Suwon 11. As shown in Figure 5, BSMV:$_{\gamma}$, BSMV:$_{\gamma}$:*Ta*ADF4, and BSMV:$_{\gamma}$:PDS (phytoene desaturase) plasmids, including a mock control (Fes buffer only) were inoculated onto wheat leaves for silencing. As expected, 9 days post-inoculation (dpi), plants inoculated with BSMV:$_{\gamma}$:PDS showed a photobleaching phenotype (Figure 5a), indicating the induction of BSMV-VIGS-mediated silencing. At this point (i.e., 9 dpi), all plants were inoculated with *Pst* CYR23 and *Pst* CYR31. In parallel, samples were collected to assess the efficiency and specificity of gene silencing by VIGS using real-time quantitative PCR analysis of *TaADF4* mRNA expression. The quantities of *TaADF4* mRNA at three sampled time points were reduced approximately 65-78% compared with the control leaves (i.e., BSMV:$_{\gamma}$) following inoculation with *Pst* CYR23 and *Pst* CYR31 at 0 hpi; this silencing was specific for *TaADF4* as the expression of none of the other 5 *ADF* genes were affected (Figure S3).

As shown in Figure 5b and 5c, we observed a significant impact on host resistance in wheat plants transformed with BSMV:$_{\gamma}$:*Ta*ADF4 at 13 dpi compared with the control leaves. Suwon 11 had a robust resistance response following *Pst* CYR23 inoculation, as evidenced by a visible necrosis on the mock and BSMV:$_{\gamma}$ control leaves. However, the *TaADF4*-knockdown wheat permitted more fungal growth, with an increase in fungal urediospores emergence on BSMV:$_{\gamma}$:*Ta*ADF4 plants (Figure 5b). Silencing of *TaADF4* did not alter the resistance response of Suwon 11 to *Pst* CYR31, which maintained wild-type-like fungal development and urediniospores reproduction phenotypes (Figure 5c). Based on these data, we conclude that *Ta*ADF4 is required for resistance to *Pst*.

Effects of _TaADF4_ silence on JA and SA accumulation

As shown Figure 4, we observed an induction in the mRNA accumulation of *TaADF4* following the exogenous application of MeJA and SA. To further confirm the relevance of *Ta*ADF4 expression as a function of the activity of JA and SA signaling pathways, we examined the relationships between *TaADF4* expression and the accumulation of JA and/or SA. To do this, we measured JA and SA levels in *TaADF4* silenced plants at 18 and 24 hours after inoculation with *Pst* CYR23. As shown in Figure 6a, we found that *TaADF4* silenced plants had reduced levels of JA, containing approximately 36-58%

of what was detected in control plants. Conversely, while SA levels in *TaADF4* silenced plants decreased approximately 17% at 18hpi, these levels increased ca. 10% at 24 hpi (Figure 6b). Taken together, we conclude that *Ta*ADF4 is required for the positive regulation of host defenses, mediated in part by JA and SA signaling.

Latrunculin-B treatment results in elevated defense responses following pathogen inoculation

Pharmacological-based approaches are an effective means to define the role of the plant actin cytoskeleton in response to numerous external stimuli, including biotic stress perception (Gibbon *et al*., 1999). To assess the impact of increased actin filament depolymerization on the response of wheat to *Pst* CYR23, we next investigated the host response via a microscopic examination of the infection process. First, we measured the accumulation of H_2O_2 at 24, 48, and 72 hpi (Figure 7a) and the development of the HR at 48, 72, and 120 hpi (Figure 7b). As shown, we observed a marked difference in both H_2O_2 accumulation and the HR between the LatB- and mock-treated leaves. For example, at 24 hpi, we rarely observed the accumulation of H_2O_2 in mesophyll cells in mock control plants, while in LatB-treated plants, H_2O_2 accumulation was frequently observed at levels significantly higher than that in mock treated samples (Figure 7a and Figure S4a). As the infection progressed, we observed a decrease in the amount of H_2O_2 accumulation in both treatments at 48 hpi (Figure 7a-ii and 7a-v), followed by an increase at 72 hpi (Figure 7a-iii and 7a-vi). These data suggests an initial pathogen-specific block in the defense response at 48 hpi, followed by the activation (i.e., recovery) of plant defense signaling at 72 hpi. In addition to an increase in H_2O_2 accumulation at 48 hpi, we also observed an increase in the HR cell death response. As shown in Figure 7b, cell death was clearly visible in LatB treated mesophyll cells; this response was reduced in mock-inoculated samples at 48 hpi and 72 hpi. Cell death was clearly observed at 120 hpi in both plants; again, however, cell death elicitation in mock-inoculated plants was significantly reduced in LatB-treated leaves (Figure 7b). There were no obvious differences between mock and LatB-treated plants in hyphal growth at 12, 24 and 48 hpi; however, hyphal lengths in mock plants were significantly longer than those observed in leaves co-inoculated with the LatB (72 hpi; Figure S4b). In addition to altered H_2O_2 accumulation, cell death and hyphal growth, qRT-PCR analyses revealed that *TaADF4* mRNA accumulation was rapidly induced, and increased significantly over time following LatB treatment, compared *TaADF4* mRNA levels in mock-treated samples (Figure 7c). Taken together, we posit that an increase in the expression of *TaADF4* is required for robust defense signaling in response to *Pst* infection.

DISCUSSION

In the current study, we identify a role for a highly conserved key regulatory node of actin cytoskeletal organization in the activation of immune signaling. In short, we demonstrate that the actin-depolymerizing factor, *Ta*ADF4 from wheat, is required for plant immunity to the stripe rust pathogen *Puccinia striiformis* f. sp. *tritici*. The data presented herein not only demonstrate that *Ta*ADF4 is an essential component of the defense response of wheat, but also that *Ta*ADF4 is required for broader stress signaling processes, including those associated with abiotic signaling and hormone perception. Thus, the current study advances our understanding of the role of the plant actin cytoskeleton during fungal pathogen infection.

In recent years, the actin cytoskeleton has emerged as a key architectural and signaling component of the eukaryotic cell, required for the activity of numerous processes, including growth and development, organelle transport and endo/exocytosis, and signaling in response to stress (Wasteneys and Galway, 2003; Hardham *et al*., 2007; Araujo-Bazán *et al*., 2008; Day *et al*., 2011). Signaling in response to biotic stress, including initial work in this area in the area of fungal pathogenesis (Kobayashi *et al*., 1994; Skalamera and Heath, 1998; Takemoto *et al.,* 2003), described a role for actin as a key structural component of the immune response, required for the localized (i.e., penetration-specific) defense signaling immediately following pathogen perception and infection. Subsequent work has led to the definition of a broader role for actin, extending beyond the initial penetration resistance response to include a more specialized function associated with signaling. The plant actin cytoskeleton has been shown to specifically respond to numerous biotic-specific stimuli – and their associated signaling processes – at multiple stages of the immune signaling cascade (Miklis *et al.,* 2007; Tian *et al*., 2009; Wang *et al*., 2009; Porter *et al*., 2012). Moreover, recent data supports a role for plant pathogenic effectors as modulators of host cytoskeletal function, either directly or indirectly targeting actin to modulate immune signaling during infection (Kang *et al*., 2014). Thus, actin represents not only a key signaling node of the plant immune platform, but also is a key target of pathogens whose organization

functions as an architectural and signaling component of cellular integrity and stimulus perception. Herein, our aim was to delineate the specificity of actin-based signaling responses and to define the modulation of host responses by virulent and avirulent fungal pathogens on wheat.

Using a combination of pharmacological and cell imaging-based approaches, rearrangement of the plant actin cytoskeleton has been correlated with the activation of defense signaling; most notably, the generation of reactive oxygen, changes in gene expression, and papillae formation at the site of penetration (Huot *et al*., 1998; Gourlay and Ayscough 2005; Wang *et al*., 2009). At the initiation of this study, we hypothesized that the plant actin cytoskeleton plays a broad, ubiquitous, role in the perception of external biotic-stress stimuli through the regulation of converging processes that regulate immune activation and defense. Indeed, the induction of *TaADF4* following exogenous MeJA application provided the initial support for our hypothesis (Figure 4). Previous work has defined the molecular-genetic and biochemical requirement for JA signaling in response to wounding, including in response to insect herbivory and necrotrophic pathogen infection (Glazebrook, 2005). Herein, we observed that the accumulation of JA was decreased in *TaADF4* silenced plants following pathogen inoculation. Taken together, these data demonstrate that JA biosynthesis is regulated by a positive feedback loop that simultaneously regulates response to growth- and defense-related processes (Howe and Jander, 2008; Melotto *et al.*, 2008).

We posit that *Ta*ADF4 – and by extension, the actin cytoskeleton – plays a fundamental role in the signaling between stimulus perception and the coordination of growth/defense signaling, *via* JA and ABA perception. Evidence in support of this hypothesis comes from numerous studies defining the mechanisms underpinning plant resistance to pathogen infection as a function of signaling processes underpinning stomata closure (Melotto *et al*., 2008; Ton *et al*., 2009) and the rapid generation of ROS in stomatal guard cells (Kwak *et al.,* 2003; Desikan *et al.,* 2004; Munemasa *et al.,* 2007; Jaspers and Kangasjärvi, 2010). Despite the demonstration of ABA as a negative regulator of post-invasive defense signaling processes, the function of ABA-dependent stomatal closure as a pre-invasive defense barrier against pathogens is well defined (Cao *et al*., 2011); moreover, it is one that requires the modulation of the plant actin cytoskeleton (Shimono *et al*., 2016a). Based on the observation of an induction in *TaADF4* following avirulent *Pst* and LatB treatments (Figures 4d and 7c), coupled with the rapid and sustained accumulation of reactive oxygen species (ROS), we conclude that *Ta*ADF4 functions, at least in part, in positively regulating pre-invasive defense against *Pst* mediated by JA and ABA signaling.

Previous work demonstrated that barley *Hv*ADF3 plays a crucial role in resistance during early stages of powdery mildew penetration (Miklis *et al*., 2007). Similarly, *Arabidopsis At*ADF4 has been shown to mediate gene-for-gene resistance activation through the modulation of mitogen-activated protein kinase (MAPK) signaling in response to perception of *Pseudomonas syringae* expressing the type-III effector AvrPphB (Tian *et al*., 2009; Porter *et al*., 2012). In the wheat-*Pst* pathosystem, a *TaADF3* knockdown wheat line showed enhanced resistance to *Pst*, suggesting that *Ta*ADF3 functions as a negative regulator of defense in response to *Pst* infection (Tang *et al*., 2015). Furthermore, previous studies have also shown that *TaADF7* is required for PR1-mediated resistance (Fu *et al*., 2014). In the current study, we show that a *Ta*ADF4-knockdown wheat line is more susceptible to the *Pst* CYR23 infection sporulation (Figure 5). Taken together with our observation of an increased expression of *Ta*ADF4 following LatB treatment, these data clearly demonstrate a role for *Ta*ADF4 as a positive regulator of immunity in response to *Pst* infection; one that results in ROS accumulation, HR cell death, and a reduction in pathogen sporulation (Figure 7). Further support for these observations come previous cytological and histological studies which observed a ROS bursts in the early infection stages (12-24 hpt) of *Pst* infection, including a concomitant change in actin cytoskeletal organization, the latter of which is a presumed early target of the oxidative burst response following pathogen infection (Huot *et al*., 1998; Gourlay and Ayscough, 2005; Wang *et al*., 2009). Our observation of LatB-induced actin filaments depolymerization, coupled with LatB-induced expression of *Ta*ADF4 following pathogen inoculation, supports a role for *Ta*ADF4 as a positive regulator of defense signaling in response to modification of the host actin cytoskeleton.

While the primary function of the ADF family of proteins is to regulate actin filament severing and depolymerization in response to changes in cellular homeostasis, our data provide a foundation in support of addressing a key gap in our understanding of ADF function: specificity. At present, the relationship(s) between the numerous ADF and ACT isoforms in plants remains undefined (Dominguez and Holmes, 2011). In *Arabidopsis*, 11 ADF isoforms have been identified. Similarly, 8 ACT isoforms exist. Previous work has demonstrated a role for ADF3 (Miklis *et al*., 2007; Tang *et al*., 2015) and ADF4 (Tian *et al*., 2009; Porter *et al*., 2012) in the activation of defense signaling following pathogen infection. However, the functional specificity of the ADF-ACT interaction remains largely undefined. Based on our observations that the expression of *TaADF4* was significantly inhibited in response to the virulent *Pst* CYR31 (Figure 4d), we posit that plant pathogens specifically target certain ADFs to modulate host responses, depending both on the nature of the pathogen (i.e., fungal versus bacterial), as well the lifestyle of the pathogen (i.e., biotrophic versus necrotrophic).

In summary, the current study demonstrates that *Ta*ADF4 positively modulates plant tolerance to stresses, likely through the regulation of downstream signaling, including the activity of JA and/or ABA signaling. While further work in this area is needed to fully define the network of cellular

processes that converge on the actin cytoskeleton during pathogen infection, the data herein further extend our understanding of the role of the ADF family of proteins. Indeed, the current study establishes a paradigm by which the function of members of the ADF family of proteins extends beyond previously demonstrated roles in penetration resistance, and support the activity of multiple intercellular signaling processes that are required for immune activation.

EXPERIMENTAL PROCEDURES

Cloning, sequencing, and phylogenetic analysis of *Ta*ADF4

A barley *ADF*-like gene was identified from GenBank (accession number AK373185), and the CDS was used as an *in silico* probe to screen the wheat EST database in GenBank using BLASTN (http://blast.ncbi.nlm.nih.gov/Blast.cgi). Conservative and homologous wheat EST sequences were extracted and assembled. To verify the assembled sequence, a pair of *TaADF4* DNA primers (Table S2) was designed to amplify the target cDNA from the wheat cultivar Suwon 11. PCR reactions were performed as follows: denaturation at 94°C for 3 min, 34 cycles (94°C for 30 sec, 50°C for 45 sec, and 72°C for 1 min), followed by 72°C for 10 min. The amplified PCR products were cloned into a pUC-T Vector (CWBIO, China), and resultant clones were sequenced (Genescript, http://www.genscript.com/).

The amino acid sequence of *TaADF4* was deduced using the online NCBI tool ORF finder (http://www.ncbi.nlm.nih.gov/gorf/gorf.html). The amino acid sequence of *TaADF4* was compared with other ADFs in GenBank using BlastP (http://blast.ncbi.nlm.nih.gov/Blast.cgi). Multiple sequence alignments were performed using ClustalW (DNASTAR, http://www.dnastar.com/). The molecular weight and theoretical isoelectric point (pI) of *TaADF4* were calculated using Protparam (http://web.expasy.org/protparam/). Phylogenetic analysis was performed using the MEGA software package (version 6.0, http://www.megasoftware.net/) using the Neighbor-Joining method. The protein domain predictions were assigned based on analysis using the SMART database (http://smart.embl-heidelberg.de). The predicted tertiary structures of *At*ADF4 and *Ta*ADF4, including the overlap model was made by SWISS-MODEL (https://swissmodel.expasy.org/interactive) and UCSF Chimera v1.11 (https://www.cgl.ucsf.edu/chimera/).

Strains and Plant Growth

Escherichia coli strains were grown on Luria Bertani (LB) medium containing antibiotics, at 37°C. *Agrobacterium tumefaciens* strain C58-C1 harboring binary vector constructs were grown on antibiotic-containing LB media at 28°C. *Saccharomyces cerevisiae* strain EGY48 carrying the plasmid p8Op:LacZ was grown on synthetic defined (SD) glucose medium lacking uracil (i.e., -Ura).

Wheat (*Triticum aestivum* L.) cv. Suwon 11 and two *Puccinia striiformis* f. sp. *tritici* (*Pst*) races, CYR23 and CYR31, were used in this study. Suwon 11 is highly resistant to *Pst* race CYR23 (infection type 0), and is highly susceptible to *Pst* race CYR31 (infection type 4) based on the reaction scale of stripe rust fungi (Stakman *et al*., 1962). *Pst* CYR23 and CYR31 urediniospores were cultured on wheat varieties Mingxian169 and Huixianhong, respectively.

Nicotiana benthamiana plants were grown at 20°C in a FLX-37 growth chamber (BioChambers, http://www.biochambers.com/) under a 16-h light/8-h dark cycle with 60% relative humidity and a light intensity of 120-mmol photons m^{-2} s^{-1}.

Plasmid Construction

The coding sequences (cDNAs) of *TaADF3*, *TaADF4*, *TaADF5*, *TaADF6*, *TaADF7*, *TaADF8*, *AtADF4*, *TaACT1* and *AtACT7* were amplified from reverse-transcribed RNA and cloned into pENTR/D-TOPO (Life Technologies, https://www.thermofisher.com/us/en/home.html) using gene-specific DNA primers (Table S2). Yeast two-hybrid prey (pB42AD) and bait (pGilda) vectors were converted into Gateway cloning-compatible pB42AD and pGilda vectors by inserting an attR cassette (Life Technologies) into the multiple cloning sites at *Eco*RI and *Xho*I. For yeast two-hybrid analyses, the *TaADF3*, *TaADF4*, *TaADF5*, *TaADF6*, *TaADF7*, *TaADF8*, *AtADF4*, *TaACT1* and *AtACT7* coding sequences from pENTR/D-TOPO (above) were recombined into pGilda-attR and pB42AD-attR using LR Clonase-II (LR Clonase; Invitrogen, https://www.thermofisher.com/) to generate C-terminal fusions to the LexA DNA binding domain and the B42 transcriptional activation domain, respectively. For co-immunoprecipitation assays, pENTR/D-TOPO expression constructs of *TaACT1* and *AtACT7* were recombined into pEarleygate203 using LR Clonase (Invitrogen, https://www.thermofisher.com/), to yield an N-terminal fusion to the Myc-epitope. T7-*TaADF4* and T7-*AtADF4* expression constructs

were created by cloning PCR-amplified cDNAs of *TaADF4* and *AtADF4* into the *Xba*I and *Sac*I restriction enzymes sites of the binary vector pMD-1 containing a N-terminal T7-epitope (Knepper *et al*., 2012).

For co-localization analysis, pENTR/D-TOPO expression constructs of *TaADF4* and *TaACT1* were recombined into pGWB555 (RFP) and pGWB505 (GFP), separately, using LR Clonase (Invitrogen, https://www.thermofisher.com/).

Yeast two-hybrid analysis

For yeast two-hybrid (Y2H) identification of protein-protein interactions, *Saccharomyces cerevisiae* strain EGY48 was co-transformed with pGilda:*At*ADF4 and pB42AD:*At*ACT7 or pGilda:*Ta*ADFs (e.g., *Ta*ADF4, *Ta*ADF3, *Ta*ADF5, *Ta*ADF6, *Ta*ADF7, or *Ta*ADF8) and pB42AD:*Ta*ACT1. pGilda:*Ta*ADFs and pGilda:*At*ADF4 protein expression in yeast were detected using anti-LexA antibody (Upstate Biotechnology, https://www.fishersci.com/us/en/home.html). Expression of pB42AD:*Ta*ACT1 and pB42AD:*At*ACT7 were detected using anti-HA antibody (Roche Life Science, https://lifescience.roche.com/). For negative controls, EGY48 was co-transformed with the empty bait vector (BD vector) and prey vector (AD vector). Transformants were selected on SD glucose plates lacking uracil (-Ura), histidine (-His), and tryptophan (-Trp). All yeast media amino acid dropout solutions were purchased from Clontech (https://www.clontech.com/).

For analysis of reporter gene activity, yeast colonies were cultured overnight in liquid synthetic defined (SD)-glucose (-Ura/-His/-Trp) medium at 30°C, harvested by centrifugation at 10,000 x *g*, and resuspended in dH_2O. The cell concentration was adjusted to an OD_{600nm} of 0.2 (ca. 2.5 x 10^6 cfu mL^{-1}). Five µL of the OD-adjusted yeast cell culture was spotted onto SD-galactose/raffinose media (-Ura/-His/-Trp/-Leu) containing 80 µg/mL X-gal. After 5-7 days at 30°C, positive interactions were identified by the presence of cell growth and a blue color.

For the Y2H *Arabidopsis* cDNA library screen, the fusion protein pGilda:*At*ADF4 or pGilda:*Ta*ADF4 was transformed into EGY48 (p8opLacZ). Transformants were selected on SD-glucose medium supplemented with an -Ura/-His dropout solution. The *Arabidopsis* cDNA library (Holt *et al*., 2002) was screened using pGilda:*At*ADF4 or pGilda:*Ta*ADF4 according to the Frozen-EZ Yeast

Transformation II Kit (Zymo Research; http://www.zymoresearch.com) protocols. The transformants were sprayed on the inducing medium [SD-galactose/raffinose containing -Ura/-His/-Trp/-Leu dropout and 80 µg ml^{-1} X-Gal]. Plates were incubated at 30°C for 7-10 days, and plasmid DNA was isolated using the Zymoprep Yeast Plasmid Miniprep II kit (Zymo Research). All plasmid inserts were verified by DNA sequencing (https://rtsf.natsci.msu.edu/).

Co-Immunoprecipitation Assays

Agrobacterium strain C58-C1 (pCH32) carrying the gene of interest expressed from the binary vector pEarleygate-203 and pMD-1 were grown overnight at 28°C on LB plates containing 100 µg/mL rifampicin, 25 µg/mL kanamycin, and 5 µg/mL tetracycline. *Agrobacterium* cells were resuspended in induction medium (10 mM MES, pH 5.6, 10 mM $MgCl_2$, and 150 µM acetosyringone) and incubated at room temperature for 2 hours before inoculation into *N. benthamiana* leaves. For Myc- and T7-tagged ACT and ADF constructs, *Agrobacterium* constructs were infiltrated at a final OD_{600nm} of 0.4. After 72 hours, *N. benthamiana* leaves (0.3 g) were harvested and ground into a powder in liquid nitrogen. Ground tissues were resuspended in 4.0mL of IP buffer (50 mM Hepes [pH 7.5], 50 mM NaCl, 10 mM EDTA, 0.2% (v/v) Triton X-100, and 1X Complete Protease Inhibitor (Roche Diagnostics, https://usdiagnostics.roche.com)). After homogenization, the crude lysates were centrifuged at 20,000 x *g* for 15 min at 4°C. Following centrifugation, 1 mL of supernatant was used for each immunoprecipitation and co-immunoprecipitation reaction. Five microliters of anti-Myc (Abcam Cambridge, MA) or anti-T7 (Novagen, http://www.emdmillipore.com) antibody was used to capture the epitope-tagged proteins. After a 1h incubation at 4°C, immunocomplexes were collected by the addition of 50 µL of protein G Sepharose-4 fast flow beads (GE Healthcare, http://www3.gehealthcare.com) and incubated end-over-end for 4 hours at 4°C. After 4 hours, immunocomplexes were washed three times with 1 mL of wash buffer (IP buffer + 0.1% (v/v) Triton X-100). After washing, the beads were resuspended in 3X SDS-PAGE loading buffer, boiled for 5 min, briefly centrifuged, and the supernatant removed for SDS-PAGE and western blot analysis.

Transient protein expression and confocal microscopy analysis

Transient protein expression assays were performed in *N. benthamiana* with *Ta*ACT1-GFP and *Ta*ADF4-RFP recombinant plasmids and empty fluorescent vector in *Agrobacterium tumefaciens* strain C58C1. Fields of epidermal pavement cells were imaged using a laser confocal scanning

microscope to collect 0.5µm interval serial sections at 54h after inoculation. Laser scanning confocal microscopy was performed with a 60x/1.42 PlanApo N objective lens on a model no. FV1000D microscope (Olympus, Melville, NY). For LatB treatment experiment, *N. benthamiana* was hand-infiltrated with 1uM LatB at 48h after induction of *Ta*ACT1-GFP or *Ta*ADF4-RFP protein. *Ta*ACT1-GFP and *Ta*ADF4-RFP were observed at 6h after LatB treatment.

Pathogen inoculation and chemical treatments

For pathogen inoculation experiments, plants were grown and inoculated following the procedure described by Kang and Li (1984). In brief, seven-day-old wheat seedlings were inoculated with fresh urediniospores of *Pst* CYR23 and CYR31. Mock inoculations were also performed using sterile water. After inoculation, plants (including the mock-inoculated plants) were kept at 100% relative humidity in the dark for 24 h, and then transferred to a growth chamber at 15°C with a 16-h light/8-h dark photoperiod. Inoculated leaves were harvested at 0, 6, 12, 18, 24, 48, and 72 h post inoculation (hpi); mock-inoculated leaves were harvested at 0 hpi.

For phytohormone treatments, wheat seedlings (7-day-old) were sprayed with 2 mM salicylic acid (SA), 100 mM abscisic acid (ABA), 100 mM ethylene (ET), and 100 mM methyl jasmonate (Me-JA), all of which were dissolved in 0.1% (v/v) ethanol. Plants treated with 0.1% (v/v) ethanol were included as a control for all hormone treatments. For high-salinity and drought-stress treatments, roots from wheat seedlings were submerged in 200 mM NaCl and 20% (w/v) PEG6000. For low- and high-temperature treatments, wheat seedlings were placed in 4°C and 37°C incubators, respectively. Wheat leaves treated with different stresses (e.g., NaCl, PEG6000, low-, and high-temperature) were harvested at 0, 1, 3, 6, 12, and 24 hours post treatment (hpt). Phytohormone-treated leaves were harvested at 0, 0.5, 3, 6, 12, and 24 hpt. Three biological replicates were performed for each treatment at each time point. All samples were flash-frozen in liquid nitrogen and stored at -80°C until RNA extraction.

BSMV-induced gene silencing

Virus-induced gene silencing (VIGS) vectors were constructed using *Barley stripe mosaic virus* according to the methods of Holzberg *et al*. (2002). The target sequence for *TaADF4*-VIGS started from the non-coding 5´ region and included approximately 350 nt of the *TaADF4* open reading frame. The resultant targeting sequence was queried using the BLASTN database

(https://blast.ncbi.nlm.nih.gov/Blast.cgi) against all available wheat sequences in the NCBI database, and the results indicated a specific targeting of only *TaADF4* in wheat. In addition, we measured *TaADF4* mRNA expression using qRT-PCR, and our results revealed a single peak by disassociation curve analysis. No additional products or polymorphisms were detected, confirming that the sequence-specific *TaADF4* RNAi could be used successfully in polyploid wheat for single gene silencing. Selected gene fragments of *TaADF4* were amplified by PCR from wheat cDNA using primers with restriction enzymes *Not*I and *Pac*I sites (Table S2). The resultant PCR products were ligated into the BSMV vector, yielding BSMV:$_\gamma$:*Ta*ADF4. To monitor silencing efficiency, plants were inoculated in parallel with BSMV:$_\gamma$ expressing phytoene desaturase (PDS; i.e., BSMV:$_\gamma$:PDS). Mock controls consisted of wheat seedlings inoculated with Fes buffer (Holzberg *et al*., 2002). Inoculations designated as BSMV:$_\gamma$ refers to the unmodified BSMV genome. Two-leaf wheat seedlings were used for virus inoculation by gently rubbing the second leaves' surface with a mixture of BSMV and Fes buffer. After virus inoculation, the seedlings were transferred to an environmentally controlled growth chamber (25°C, 16-h light/8-h dark photoperiod). Photobleaching symptoms in the PDS control plants were observed 9 days after virus inoculation. The fourth leaves of plants were inoculated with *Pst* races CYR23 and CYR31, separately, and sampled at 0, 24, and 48 hpi and processed for qRT-PCR to assess silencing efficiency. Infection phenotypes were observed 13 dpi. Three biological replicates were performed.

Quantification of jasmonic acid and salicylic acid by liquid chromatography-tandem mass spectrometry (LC-MS)

TaADF4 silenced and control seedlings (ca. 250 mg) were collected at 18 and 24 hours after inoculation with *Pst* CYR23 and were flash-frozen in liquid N_2. Frozen samples were ground under liquid N_2 with a mortar and pestle, and the fine powder was extracted with 1 mL MeOH-H_2O-HOAc (90:9:1, v/v/v) and centrifuged 1 min at 10,000 rpm. The extraction was repeated twice with 500 µl of same extraction buffer. The three extractions (supernatants) were combined and dried under N_2 gas, then resuspended in 800 µl of 100% MeOH. The resuspended samples were then filtered through a 0.2 mm PTFE membrane (Millipore, Bedford, MA). Quantitation was performed by Quattro Premier XE tandem quadrupole mass spectrometer (Waters Corporation, Milford, MA). Peak areas were integrated, and the analytes were quantified based on standard curves generated from peak area ratios of analytes related to the corresponding internal standard.

Inhibition treatment and histological observation

Latrunculin-B (LatB; Sigma-Aldrich, https://www.sigmaaldrich.com/) was used at a final concentration of 1 μM dissolved in 0.01% (v/v) DMSO. Mock treatment was 0.01% (v/v) DMSO. First, the tip of a syringe was pressed against the abaxial surface of two-week-old wheat leaves, and the LatB solution (300-400 μL) was forced into the apoplast under gentle pressure, as previously described (Yun *et al*., 2003). The treated and mock wheat leaves were rinsed three times using sterile water and then inoculated with fresh urediniospores of CYR23. Leaves were harvested at 0, 6, 12, 24, 48 and 72 hpi, frozen in liquid nitrogen, and stored at -80°C until RNA extraction.

To quantify H_2O_2 accumulation and the induction of HR cell death during *Pst* infection, 3,3-diaminobenzidine (DAB) and trypan blue staining were performed following the method of Thordal-Christensen *et al*. (1997), viewed under differential interference contrast (DIC) optics, and data were analyzed using the DP-BSW software package (Olympus, http://www.olympus-lifescience.com). All microscopic examinations were performed using a Nikon Eclipse 80i microscope equipped with DIC (Nikon Corporation, http://www.nikon.com/). At least 50 penetration sites on each of four leaf samples were observed at each time point. The infection phenotypes of wheat leaves were observed at 15 dpi.

Quantitative RT-PCR analysis

Quantitative real-time PCR (qRT-PCR) was performed using the iQ5 Real-Time PCR Detection System (Bio-Rad, http://www.bio-rad.com/). DNA primers of *Ta*ADF3, *Ta*ADF4, *Ta*ADF5, *Ta*ADF6, *Ta*ADF7, *Ta*ADF8 for qRT-PCR were designed Primer Premier v5.0. Elongation factor-1 alpha (*EF-1h*) was used as an internal control for qRT-PCR. All DNA primers used for qRT-PCR are listed in Table S2. The 2X UltraSYBR Green Mix (CWBIO, China) was used in 25 μL PCR reaction volumes. The qRT-PCR cycling program was as follows: 95°C for 10 min, followed by 40 cycles (15 sec at 95°C, 30 sec at 54.5°C and 30 sec at 72°C). All samples were subjected to melt curve analysis between 55°C and 95°C to determine the accuracy and specificity of the reaction. Non-template control reactions (i.e., no cDNA) were performed in parallel. The standard curve was constructed using five serial dilutions (e.g., 5^{-1}, 5^{-2}, 5^{-3}, 5^{-4} and 5^{-5}) as compared to mock-inoculated wheat leaf samples harvested at 0 hpi. The correlation coefficient of the analysis was greater than 0.99. The relative expression of the target gene was calculated using the comparative Ct method with the formula $2^{-\Delta\Delta CT}$-[ΔΔCT = ΔCT

(test) - ΔCT (calibrator)]. Three independent replicates were performed at each time point. Statistical analysis was performed using two-tailed analysis of variance (ANOVA) with the SPSS 17.0 program (IBM SPSS Statistics, https://www.ibm.com/marketplace/cloud/statistical-analysis-and-reporting/us/en-us). A value of $P < 0.05$ indicates a significant difference between two groups.

ACKNOWLEDGMENTS

We thank Amy Baetsen-Young, Alex Corrion, and Yi-Ju Lu for critical reading of the manuscript, as well as helpful suggestions throughout the completion of this study. BZ was supported by a fellowship from the China Scholarship Council. Research in the lab of Brad Day was supported by a grant from the United States National Science Foundation (IOS-1021044). Research presented herein was supported by the National Natural Science Foundation of China (Grant No. 31272024 and 31571960), and the 111 Project from the Ministry of Education of China (Grant No. B07049). The authors declare no conflicts of interest.

SHORT SUPPORTING INFORMATION LEGENDS

Figure S1. ADF4 and ACT interactions identified by yeast two-hybrid screening.

Figure S2. Laser-scanning confocal micrographs showing fluorescence of leaf cells expressing GFP alone, *Ta*ADF4-RFP (top), and RFP alone and *Ta*ACT1-GFP (bottom).

Figure S3. Relative expression of *TaADF4* mRNA in Suwon 11 leaves after gene silencing.

Figure S4. H_2O_2 accumulation and *Pst* hyphal growth following LatB treatment.

Table S1. Protein interactions between *At*ADF4 and *Ta*ADF4 identified from the yeast two-hybrid library screen.

Table S2. DNA primers used in this study.

REFERENCES

Akin, B., Chen, X.M., Morgounov, A., Zencirci, N., Wan, A. and Wang, M. (2016) High-temperature adult-plant (HTAP) stripe rust (*Puccinia striiformis* f. sp. *tritici*) resistance in facultative winter wheat. *Crop Pasture Sci*. *In press*.

Araujo-Bazán, L., Peñalva, M.A. and Espeso, E.A. (2008) Preferential localization of the endocytic internalization machinery to hyphal tips underlies polarization of the actin cytoskeleton in *Aspergillus nidulans*. *Mol. Microbiol.*, **67**, 891-905.

Beddow, J.M., Pardey, P.G., Chai, Y., Hurley, T.M., Kriticos, D.J., Braun, H.J., Park, R.F., Cuddy, W.S. and Yonow, T. (2015) Research investment implications of shifts in the global geography of wheat stripe rust. *Nat. Plant*, **1**, 15132.

Bennypaul, H.S., Mutti, J.S., Rustgi, S., Kumar, N., Okubara, P.A. and Gill, K.S. (2012) Virus-induced gene silencing (VIGS) of genes expressed in root, leaf, and meiotic tissues of wheat. *Funct. Integr. Genomics*, **12**, 143-156.

Cao, F.Y., Yoshioka, K. and Desveaux, D. (2011) The roles of ABA in plant-pathogen interactions. *J. Plant Res.*, **124**, 489-499.

Chen, C.W., Yang, Y.W., Lur, H.S., Tsai, Y.G. and Chang, M.C. (2006) A novel function of abscisic acid in the regulation of rice (*Oryza sativa* L.) root growth and development. *Plant Cell Physiol.*, **47**, 1-13.

Chen, W., Wellings, C., Chen, X., Kang, Z. and Liu, T. (2014) Wheat stripe (yellow) rust caused by *Puccinia striiformis* f. sp. *tritici*. *Mol. Plant Pathol.*, **15**, 433-446.

Chen, X. (2005) Epidemiology and control of stripe rust [*Puccinia striiformis* f. sp. *tritici*] on wheat. *Can. J. Plant Pathol.*, **27**, 314-337.

Chen, X.M., Moore, M., Milus, E.A., Long, D.L., Line, R.F., Marshall, D. and Jackson, L. (2002) Wheat stripe rust epidemics and races of *Puccinia striiformis* f. sp. *tritici* in the United States in 2000. *Plant Dis.*, **86**, 39-46.

Chisholm, S.T., Coaker, G., Day, B. and Staskawicz, B.J. (2006) Host-microbe interactions: shaping the evolution of the plant immune response. *Cell*, **124**, 803-814.

Day, B., Henty, J.L., Porter, K.J. and Staiger, C.J. (2011) The pathogen-actin connection: a platform for defense signaling in plants. *Ann. Rev. Phytopathol.*, **49**, 483-506.

Desikan, R., Cheung, M.K., Bright, J., Henson, D., Hancock, J.T. and Neill, S.J. (2004) ABA, hydrogen peroxide and nitric oxide signalling in stomatal guard cells. *J. Exp. Bot.*, **55**, 205-212.

Dominguez, R. and Holmes, K.C. (2011) Actin structure and function. *Ann. Rev. Biophys.*, **40**, 169.

Fu, Y., Duan, X., Tang, C., Li, X., Voegele, R.T., Wang, X., Wei, G. and Kang, Z. (2014) TaADF7, an actin-depolymerizing factor, contributes to wheat resistance against *Puccinia striiformis* f. sp. *tritici*. *Plant J.*, **78**, 16-30.

Gibbon, B.C., Kovar, D.R. and Staiger, C.J. (1999) Latrunculin B has different effects on pollen germination and tube growth. *Plant cell*, **11**, 2349-2363.

Gilliland, L.U., Pawloski, L.C., Kandasamy, M.K. and Meagher, R.B. (2003) *Arabidopsis* actin gene *ACT7* plays an essential role in germination and root growth. *Plant J.*, **33**, 319-328.

Glazebrook, J. (2005) Contrasting mechanisms of defense against biotrophic and necrotrophic pathogens. *Annu. Rev. Phytopathol.*, **43**, 205-227.

Gourlay, C.W. and Ayscough, K.R. (2005) Identification of an upstream regulatory pathway controlling actin-mediated apoptosis in yeast. *J. Cell Sci.*, **118**, 2119-2132.

Hardham, A.R., Jones, D.A. and Takemoto, D. (2007) Cytoskeleton and cell wall function in penetration resistance. *Curr. Opin. Plant Biol.*, **10**, 342-348.

Henty-Ridilla, J.L., Shimono, M., Li, J., Chang, J.H., Day, B. and Staiger, C.J. (2013) The plant actin cytoskeleton responds to signals from microbe-associated molecular patterns. *PLoS Pathog.*, **9**, e1003290.

Holt, B.F., Boyes, D.C., Ellerström, M., Siefers, N., Wiig, A., Kauffman, S., Grant, M.R. and Dangl, J.L. (2002) An evolutionarily conserved mediator of plant disease resistance gene function is required for normal *Arabidopsis* development. *Dev. Cell*, **2**, 807-817.

Holzberg, S., Brosio, P., Gross, C. and Pogue, G.P. (2002) Barley stripe mosaic virus-induced gene silencing in a monocot plant. *Plant J.*, **30**, 315-327.

Hovmøller, M.S., Walter, S. and Justesen, A.F. (2010) Escalating threat of wheat rusts. *Science*, **329**, 369-369.

Howe, G.A. and Jander, G. (2008) Plant immunity to insect herbivores. *Annu. Rev. Plant Biol.*, **59**, 41-66.

Huang, G.T., Ma, S.L., Bai, L.P., Zhang, L., Ma, H., Jia, P., Liu, J., Zhong, M. and Guo, Z.F. (2012) Signal transduction during cold, salt, and drought stresses in plants. *Mol. Biol. Rep.*, **39**, 969-987.

Huang, S., An, Y.Q., McDowell, J.M., McKinney, E.C. and Meagher, R.B. (1997) The *Arabidopsis* ACT11 actin gene is strongly expressed in tissues of the emerging inflorescence, pollen, and developing ovules. *Plant Mol. Biol.*, **33**, 125-139.

Huot, J., Houle, F., Rousseau, S., Deschesnes, R.G., Shah, G.M. and Landry, J. (1998) SAPK2/p38-dependent F-actin reorganization regulates early membrane blebbing during stress-induced apoptosis. *J. Cell Biol.*, **143**, 1361-1373.

Inada, N., Higaki, T. and Hasezawa, S. (2016) Nuclear Function of Subclass I Actin-Depolymerizing Factor Contributes to Susceptibility in *Arabidopsis* to an Adapted Powdery Mildew Fungus. *Plant Physiol.*, **170**, 1420-1434.

Jaspers, P. and Kangasjärvi, J. (2010) Reactive oxygen species in abiotic stress signaling. *Physiol. Plantarum*, **138**, 405-413.

Jin, Y., Szabo, L.J. and Carson, M. (2010) Century-old mystery of *Puccinia striiformis* life history solved with the identification of *Berberis* as an alternate host. *Phytopathol.*, **100**, 432-435.

Jones, J.D. and Dangl, J.L. (2006) The plant immune system. *Nature*, **444**, 323-329.

Kandasamy, M.K., Gilliland, L.U., McKinney, E.C. and Meagher, R.B. (2001) One plant actin isovariant, ACT7, is induced by auxin and required for normal callus formation. *Plant Cell*, **13**, 1541-1554.

Kang, Y., Jelenska, J., Cecchini, N.M., Li, Y., Lee, M.W., Kovar, D.R. and Greenberg, J.T. (2014) HopW1 from *Pseudomonas syringae* disrupts the actin cytoskeleton to promote virulence in *Arabidopsis*. *PLoS Pathog.*, **10**, e1004232.

Kang, Z.S., Huang, L.L., Buchenauer, H. (2002) Ultrastructural changes and localization of lignin and callose in compatible and incompatible interactions between wheat and *Puccinia striiformis*. *Z. Pflanzenkr Pflanzenschutz* **109**, 25-37.

Kang, Z. and Li, Z. (1984) Discovery of a normal T. type new pathogenic strain to Lovrin10. *Acta Coll Septentr Occident Agric*. **4**,18-28.

Knepper C, Day B (2010) From perception to activation: The molecular-genetic and biochemical landscape of disease resistance signaling in plants. *The Arabidopsis Book,*1-17.

Kobayashi, I., Kobayashi, Y. and Hardham, A.R. (1994) Dynamic reorganization of microtubules and microfilaments in flax cells during the resistance response to flax rust infection. *Planta*, **195**, 237-247.

Kobayashi, Y., Kobayashi, I., Funaki, Y., Fujimoto, S., Takemoto, T. and Kunoh, H. (1997) Dynamic reorganization of microfilaments and microtubules is necessary for the expression of non-host resistance in barley coleoptile cells. *Plant J.*, **11**, 525-537.

Kwak, J.M., Mori, I.C., Pei, Z.M., Leonhardt, N., Torres, M.A., Dangl, J.L., Bloom, R.E., Bodde, S., Jones, J.D. and Schroeder, J.I. (2003) NADPH oxidase *AtrbohD* and *AtrbohF* genes function in ROS-dependent ABA signaling in *Arabidopsis*. *EMBO J.*, **22**, 2623-2633.

Lappalainen, P. and Drubin, D.G. (1997) Cofilin promotes rapid actin filament turnover *in vivo*. *Nature*, **388**, 78-82.

McDowell, J.M., An, Y., Huang, S., McKinney, E.C. and Meagher, R.B. (1996) The *Arabidopsis* ACT7 actin gene is expressed in rapidly developing tissues and responds to several external stimuli. *Plant Physiol.*, **111**, 699-711.

Melotto, M., Mecey, C., Niu, Y., Chung, H.S., Katsir, L., Yao, J., Zeng, W., Thines, B., Staswick, P. and Browse, J. (2008) A critical role of two positively charged amino acids in the Jas motif of *Arabidopsis* JAZ proteins in mediating coronatine- and jasmonoyl isoleucine-dependent interactions with the COI1 F-box protein. *Plant J.*, **55**, 979-988.

Miklis, M., Consonni, C., Bhat, R.A., Lipka, V., Schulze-Lefert, P. and Panstruga, R. (2007) Barley MLO modulates actin-dependent and actin-independent antifungal defense pathways at the cell periphery. *Plant Physiol.*, **144**, 1132-1143.

Milus, E.A., Kristensen, K. and Hovmøller, M.S. (2009) Evidence for increased aggressiveness in a recent widespread strain of *Puccinia striiformis* f. sp. *tritici* causing stripe rust of wheat. *Phytopathol.*, **99**, 89-94.

Munemasa, S., Oda, K., Watanabe-Sugimoto, M., Nakamura, Y., Shimoishi, Y. and Murata, Y. (2007) The coronatine-insensitive 1 mutation reveals the hormonal signaling interaction between abscisic acid and methyl jasmonate in *Arabidopsis* guard cells. Specific impairment of ion channel activation and second messenger production. *Plant Physiol.*, **143**, 1398-1407.

Ouellet, F., Carpentier, E., Cope, M.J.T., Monroy, A.F. and Sarhan, F. (2001) Regulation of a wheat actin-depolymerizing factor during cold acclimation. *Plant Physiol.*, **125**, 360-368.

Plett, J.M., Mathur, J. and Regan, S. (2009) Ethylene receptor ETR2 controls trichome branching by regulating microtubule assembly in *Arabidopsis thaliana*. *J. Exp. Bot.,*e228.

Porter, K., Shimono, M., Tian, M. and Day, B. (2012) *Arabidopsis* Actin-Depolymerizing Factor-4 links pathogen perception, defense activation and transcription to cytoskeletal dynamics. *PLoS Pathog.*, **8**, e1003006.

Ruzicka, D.R., Kandasamy, M.K., McKinney, E.C., Burgos-Rivera, B. and Meagher, R.B. (2007) The ancient subclasses of *Arabidopsis* Actin Depolymerizing Factor genes exhibit novel and differential expression. *Plant J.*, **52**, 460-472.

Schmidt, S.M. and Panstruga, R. (2007) Cytoskeleton functions in plant-microbe interactions. *Physiol Mol. Plant Pathol.*, **71**, 135-148.

Schultz, J., Milpetz, F., Bork, P. and Ponting, C.P. (1998) SMART, a simple modular architecture research tool: identification of signaling domains. *Proc. Natl. Acad. Sci. U S A*, **95**, 5857-5864.

Scofield, S.R., Huang, L., Brandt, A.S. and Gill, B.S. (2005) Development of a virus-induced gene-silencing system for hexaploid wheat and its use in functional analysis of the Lr21-mediated leaf rust resistance pathway. *Plant Physiol.*, **138**, 2165-2173.

Sharma-Poudyal, D., Chen, X., Wan, A., Zhan, G., Kang, Z., Cao, S., Jin, S., Morgounov, A., Akin, B. and Mert, Z. (2013) Virulence characterization of international collections of the wheat stripe rust pathogen, *Puccinia striiformis* f. sp. *tritici*. *Plant Dis.* **97**, 379-386.

Shimada, C., Lipka, V., O'Connell, R., Okuno, T., Schulze-Lefert, P. and Takano, Y. (2006) Nonhost resistance in *Arabidopsis*-Colletotrichum interactions acts at the cell periphery and requires actin filament function. *Mol. Plant Microbe Interact.*, **19**, 270-279.

Shimono, M., Higaki, T., Kaku, H., Shibuya, N., Hasezawa, S. and Day, B. (2016a) Quantitative evaluation of stomatal cytoskeletal patterns during the activation of immune signaling in *Arabidopsis thaliana*. *PloS One*, **11**, e0159291.

Shimono, M., Lu, Y., Porter, K., Kvitko, B., Creason, A., Henty-Ridilla, J., He, S.Y., Chang, J.H., Staiger, C. and Day, B. (2016b). The *Pseudomonas syringae* type III effector HopG1 induces actin filament remodeling in Arabidopsis in association with disease symptom development. *Plant Physiol*., ***171, 2239-2255.***

Skalamera, D. and Heath, M.C. (1998) Changes in the cytoskeleton accompanying infection-induced nuclear movements and the hypersensitive response in plant cells invaded by rust fungi. *Plant J.*, **16**, 191-200.

Šlajcherová, K., Fišerová, J., Fischer, L. and Schwarzerová, K. (2012) Multiple actin isotypes in plants: diverse genes for diverse roles? *Front. Plant Sci.*, **3**, 226.

Stakman, E.C., Stewart, D. and Loegering, W.Q. (1962) Identification of physiologic races of *Puccinia graminis* var. *tritici*. Agric. Res. Serv., U.S. Dept. Agric. *E617* (revised).

Stamnes, M. (2002) Regulating the actin cytoskeleton during vesicular transport. *Curr. Opin. Cell Biol.*, **14**, 428-433.

Takahashi, H., Kawahara, A. and Inoue, Y. (2003) Ethylene promotes the induction by auxin of the cortical microtubule randomization required for low-pH-induced root hair initiation in lettuce (*Lactuca sativa L*.) seedlings. *Plant cell Physiol.*, **44**, 932-940.

Takemoto, D. and Hardham, A.R. (2004) The cytoskeleton as a regulator and target of biotic interactions in plants. *Plant Physiol.*, **136**, 3864-3876.

Takemoto, D., Jones, D.A. and Hardham, A.R. (2003) GFP-tagging of cell components reveals the dynamics of subcellular re-organization in response to infection of *Arabidopsis* by oomycete pathogens. *Plant J.*, **33**, 775-792.

Tang, C., Deng, L., Chang, D., Chen, S., Wang, X. and Kang, Z. (2015) TaADF3, an Actin-Depolymerizing Factor, Negatively Modulates Wheat Resistance Against *Puccinia striiformis*. *Front. Plant Sci.*, **6**, 1214.

Thordal-Christensen, H., Zhang, Z., Wei, Y. and Collinge, D.B. (1997) Subcellular localization of H_2O_2 in plants. H_2O_2 accumulation in papillae and hypersensitive response during the barley-powdery mildew interaction. *Plant J.*, **11**, 1187-1194.

Tian, M., Chaudhry, F., Ruzicka, D.R., Meagher, R.B., Staiger, C.J. and Day, B. (2009) *Arabidopsis* actin-depolymerizing factor AtADF4 mediates defense signal transduction triggered by the *Pseudomonas syringae* effector AvrPphB. *Plant Physiol.*, **150**, 815-824.

Ton, J., Flors, V. and Mauch-Mani, B. (2009) The multifaceted role of ABA in disease resistance. *Trends Plant Sci.*, **14**, 310-317.

Wang, C.F., Huang L.L., Buchenauer H, Han, Q.M., Zhang, H.C., Kang, Z.S. (2007) Histochemical studies on the accumulation of reactive oxygen species (O^{-2} and H_2O_2) in the incompatible and compatible interaction of wheat - *Puccinia striiformis* f. sp *tritici*. *Physiol. Mol. Plant Pathol.* **71**, 230-239.

Wang, N., Tytell, J.D. and Ingber, D.E. (2009) Mechanotransduction at a distance: mechanically coupling the extracellular matrix with the nucleus. *Nat. Rev. Mol. Cell Biol.*, **10**, 75-82.

Wasteneys, G.O. and Galway, M.E. (2003) Remodeling the cytoskeleton for growth and form: an overview with some new views. *Annu.Rev. Plant Biol.*, **54**, 691-722.

Yan, S., Tang, Z., Su, W. and Sun, W. (2005) Proteomic analysis of salt stress-responsive proteins in rice root. *Proteomics*, **5**, 235-244.

Yun, B.W., Atkinson, H.A., Gaborit, C., Greenland, A., Read, N.D., Pallas, J.A. and Loake, G.J. (2003) Loss of actin cytoskeletal function and EDS1 activity, in combination, severely compromises non-host resistance in *Arabidopsis* against wheat powdery mildew. *Plant J.*, **34**, 768-777.

Zhao, J., Zhang, H., Yao, J., Huang, L. and Kang, Z. (2011) Confirmation of *Berberis* spp. as alternate hosts of *Puccinia striiformis* f. sp. *tritici* on wheat in China. *Mycosystema*, **30**, 895-900.

FIGURE LEGENDS

Figure 1. Sequence and structure analysis of wheat actin depolymerizing factor-4 protein.

(a) Multiple protein sequence alignment of *Ta*ADF4 and characterized members of the plant family of ADF proteins. Amino acid similarity plot (shown above alignments): red column indicates the highest amino acid sequence similarity, followed by orange, green and blue. Individual amino acid residue shading is as follows: Red, residues that match the consensus within 10; yellow, residues that match the consensus within 5; green, residues that match the consensus exactly.

(b) Evolutionary analysis of *Ta*ADF4. Analysis was conducted using the Neighbor-Joining method in MEGA6.0. Branches are labeled with protein names and GenBank accession numbers. Representative phylogenetic tree of *Ta*ADF4 and ADF family member proteins from *Secale cereale* × *Triticum durum* (*Sc* × *Td*), *Oryza sativa* (*Os*ADF), *Zea mays* (*Zm*ADF), *Arabidopsis thaliana* (*At*ADF). GenBank accession numbers are shown after the gene names. The red rhombus represents *Triticum aestivum* L. (*Ta*ADF4).

(c) Predicted domain architecture of *Ta*ADF4. The *TaADF4* CDS encodes a 139 amino acids containing one ADF domain (amino acids 6-138), five F-actin binding sites (amino acids 82, 84, 98, 125, and 128), and two G-actin binding sites (amino acids 6 and 7). Six additional motifs were also identified, including three predicted protein kinase C phosphorylation sites (amino acids 26-28, 94-96, and 105-107), two casein kinase II phosphorylation sites (amino acids 52-55 and 105-108), and one N-myristoylation site (amino acids 7-12).

(d) Predicted tertiary structure and homology modeling of *Ta*ADF4 and *At*ADF4. The cyan ribbon represents the model of *Ta*ADF4 and the beige ribbon is *At*ADF4.

Figure 2. ADF and ACT physically interact *in planta*.

(a) Yeast two-hybrid assay identification of an *in vivo* interaction between *At*ADF4 and *At*ACT7 (left) and *Ta*ADF4 and *Ta*ACT1 (right).

(b) ADF4 and ACT proteins interact *in planta*. *Agrobacterium* strains containing epitope-tagged expression constructs of *At*ADF4 and *At*ACT7 (top blots) or *Ta*ADF4 and *Ta*ACT1 were transiently

expressed in *N. benthamiana*. Anti-Myc and anti-T7 immunoprecipitated proteins were isolated 72 h after inoculation. Protein sizes are indicated at the left side of the immunoblots.

(c) *In vivo* interaction between *Ta*ADFs and *Ta*ACT1. Yeast cells were grown on galactose dropout media containing X-gal (-Ura/-His/-Trp/-Leu). Negative control yeast strains contained the pGilda (BD) vector or the pB42AD (AD) vector.

(d) Predicted tertiary homology modeling of *Ta*ADF3, *Ta*ADF4, *Ta*ADF5, *Ta*ADF6, *Ta*ADF7 and *Ta*ADF8. The beige ribbon represents *Ta*ADF3, red is *Ta*ADF4, grey is *Ta*ADF5, blue is *Ta*ADF7, green is *Ta*ADF6, and purple is *Ta*ADF8.

Figure 3. *Ta*ADF4 localizes to actin filaments.

(a) Images of transiently expressed *Ta*ACT1-GFP and *Ta*ADF4-RFP in *Nicotiana benthamiana* were taken by laser scanning confocal microscopy. Bar = 10 µm.

(b) LatB treatment of cells expressing *Ta*ADF4-RFP and *Ta*ACT1-GFP results in filament depolymerization and dissociation of *Ta*ADF4-RFP from F-actin structures. Bar = 10 µm.

Figure 4. *TaADF4* mRNA accumulation is induced in response to hormone treatment, abiotic, and biotic stress perception.

(a) Real-time PCR analysis of *TaADF4* mRNA accumulation from various wheat tissue types.

(b) *Ta*ADF4 expression is induced following abscisic acid (ABA) and methyl-JA (JA) perception. qRT-PCR analysis of *TaADF4* mRNA accumulation in leaves of Suwon 11 following hormone treatment. Leaves were treated with, individually, ethylene (ET), methyl-JA, ABA, and salicylic acid (SA), and samples were collected at 0-24 hours post-treatment (hpt). * Indicates statistically significant difference between incompatible and compatible interactions ($P < 0.05$). All data were normalized using the internal control expression of *TaEF-1α*. Error bars represent the standard deviation of expression from three independent biological replicates.

(c) *TaADF4* is rapidly induced in response to high-temperature, and down-regulated in response to drought, low-temperature, and salinity. qRT-PCR analysis of *TaADF4* mRNA accumulation in response to abiotic stress perception. Suwon 11 leaves were stimulated with PEG6000 (drought simulation), high-temperature (HT), low-temperature (LT), and high salinity (NaCl), and mRNA expression was quantified at time intervals between 0 and 24 hpt. * Indicates statistically significant difference

between incompatible and compatible interactions ($P < 0.05$). All data were normalized using the internal control expression of *TaEF-1α*. Error bars represent the standard deviation of expression from three independent biological replicates.

(d) *TaADF4* mRNA expression is rapidly induced in response to inoculation with the virulent *Pst* strain CYR23. qRT-PCR analysis of *TaADF4* mRNA accumulation in Suwon 11 leaves after inoculation with *Pst* CYR23 (incompatible) and *Pst* CYR31 (compatible). * Indicates statistically significant difference between incompatible and compatible interactions ($P < 0.05$). All data were normalized using the internal control expression of *TaEF-1α*. Error bars represent the standard deviation of expression from three independent biological replicates.

Figure 5. Silencing of *Ta*ADF4 in wheat renders plants susceptible to *Pst* CYR23.

Infection phenotypes of mock, BSMV:$_\gamma$, BSMV:$_\gamma$:PDS, and BSMV:$_\gamma$:*TaADF4* wheat leaves at 15 dpi.

(a) Control wheat lines, consisting of mock- (Fes buffer), BSMV:$_\gamma$-, and BSMV:$_\gamma$:PDS-transformed lines. No pathogen inoculation.

(b) Mock-, BSMV:$_\gamma$-, and BSMV:$_\gamma$:*TaADF4*-transformed lines inoculated with *Pst* CYR23.

(c) Mock-, BSMV:$_\gamma$-, and BSMV:$_\gamma$:*TaADF4*-transformed lines inoculated with *Pst* CYR31.

Figure 6. Jasmonic acid levels are reduced in *Pst* CYR23-inoculated *TaADF4* silenced plants.

(a) Jasmonic Acid (JA) levels after plants inoculated with *Pst* CYR23 at 18 and 24 hpi.

(b) Salicylic acid (SA) levels remain unchanged in *TaADF4* silenced plants following inoculation with *Pst* CYR23 at 18 and 24 hpi. Data shown is from three biological replicates. Error bars represent the standard deviation of expression from three independent biological replicates. * Indicates statistically significant differences in JA accumulation between WT and *TaADF4* RNAi-silenced plants ($P < 0.05$).

Figure 7. Treatment of wheat leaves with latrunculin-B enhances defense responses and abrogates *Pst* infection.

(a) Histological observation of H_2O_2 accumulation in mock treatment (i-iii) and LatB-treated (iv-vi) wheat leaves inoculated with *Pst* CYR23.

(b) Histological observation of hypersensitive cell death in wheat leaves inoculated with *Pst* CYR23. i-iii, mock. iv-vi, LatB treatment. Blue (trypan) staining indicates hypersensitive cell death. SP, spore; GT, germ tube; SV, sub-stomatal vesicle; HMC, haustorial mother cell; IH, infection hypha; HR, hypersensitive response. Bar = 25 μm.

(c) The expression level of *TaADF4* mRNA in Suwon 11 leaves following infiltration with LatB, and mock-inoculation. * Indicates statistically significant differences between treatments ($P < 0.05$). All data were normalized to *TaEF-1α* expression levels. Error bars represent the standard deviation of expression from three independent biological replicates.

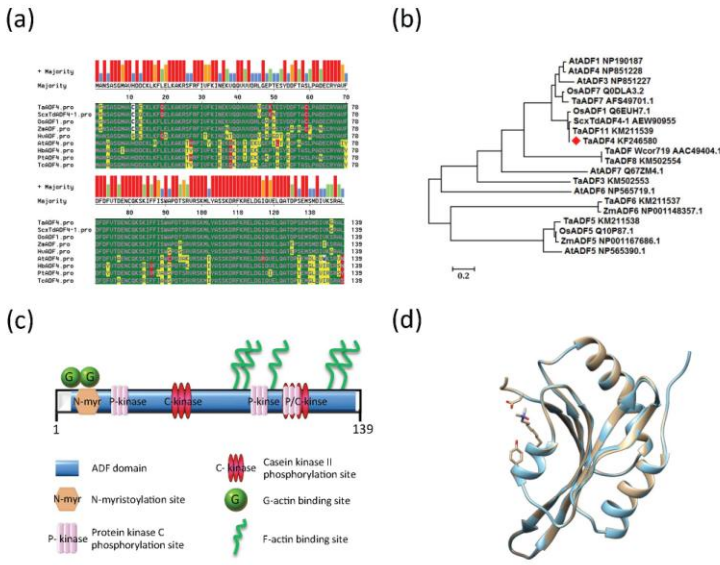

Figure 1. Sequence and structure analysis of wheat actin depolymerizing factor-4 protein.

(a) Multiple protein sequence alignment of *Ta*ADF4 and characterized members of the plant family of ADF proteins. Amino acid similarity plot (shown above alignments): red column indicates the highest amino acid sequence similarity, followed by orange, green and blue. Individual amino acid residue shading is as follows: Red, residues that match the consensus within 10; yellow, residues that match the consensus within 5; green, residues that match the consensus exactly.

(b) Evolutionary analysis of *Ta*ADF4. Analysis was conducted using the Neighbor-Joining method in MEGA6.0. Branches are labeled with protein names and GenBank accession numbers. Representative phylogenetic tree of *Ta*ADF4 and ADF family member proteins from *Secale cereale* × *Triticum durum* (*Sc* × *Td*), *Oryza sativa* (*Os*ADF), *Zea mays* (*Zm*ADF), *Arabidopsis thaliana* (*At*ADF). GenBank accession numbers are shown after the gene names. The red rhombus represents *Triticum aestivum* L. (*Ta*ADF4).

(c) Predicted domain architecture of *Ta*ADF4. The *TaADF4* CDS encodes a 139 amino acids containing one ADF domain (amino acids 6-138), five F-actin binding sites (amino acids 82, 84, 98, 125, and 128), and two G-actin binding sites (amino acids 6 and 7). Six additional motifs were also identified, including three predicted protein kinase C phosphorylation sites (amino acids 26-28, 94-96, and 105-107), two casein kinase II phosphorylation sites (amino acids 52-55 and 105-108), and one N-myristoylation site (amino acids 7-12).

(d) Predicted tertiary structure and homology modeling of *Ta*ADF4 and *At*ADF4. The cyan ribbon represents the model of *Ta*ADF4 and the beige ribbon is *At*ADF4.

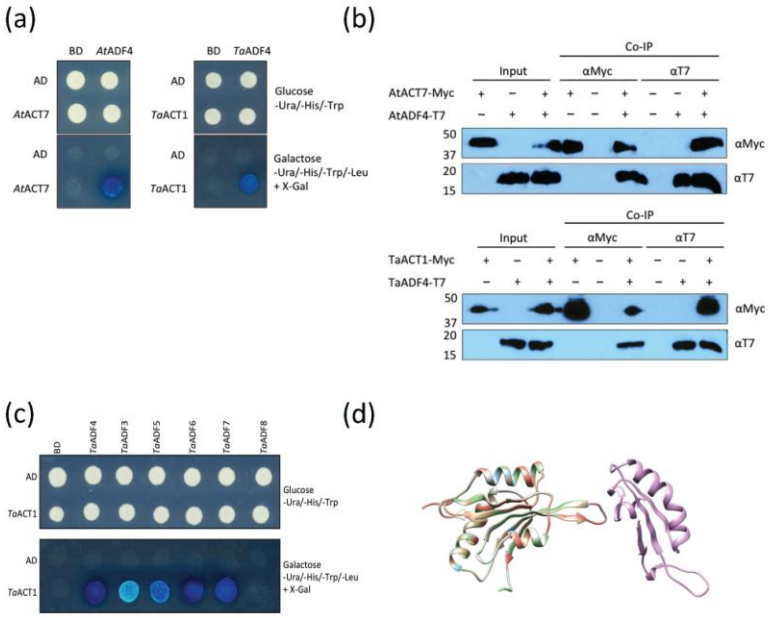

Figure 2. ADF and ACT physically interact *in planta*.
(a) Yeast two-hybrid assay identification of an *in vivo* interaction between *At*ADF4 and *At*ACT7 (left) and *Ta*ADF4 and *Ta*ACT1 (right).
(b) ADF4 and ACT proteins interact *in planta*. *Agrobacterium* strains containing epitope-tagged expression constructs of *At*ADF4 and *At*ACT7 (top blots) or *Ta*ADF4 and *Ta*ACT1 were transiently expressed in *N. benthamiana*. Anti-Myc and anti-T7 immunoprecipitated proteins were isolated 72 h after inoculation. Protein sizes are indicated at the left side of the immunoblots.
(c) *In vivo* interaction between *Ta*ADFs and *Ta*ACT1. Yeast cells were grown on galactose dropout media containing X-gal (-Ura/-His/-Trp/-Leu). Negative control yeast strains contained the pGilda (BD) vector or the pB42AD (AD) vector.
(d) Predicted tertiary homology modeling of *Ta*ADF3, *Ta*ADF4, *Ta*ADF5, *Ta*ADF6, *Ta*ADF7 and *Ta*ADF8. The beige ribbon represents *Ta*ADF3, red is *Ta*ADF4, grey is *Ta*ADF5, blue is *Ta*ADF7, green is *Ta*ADF6, and purple is *Ta*ADF8.

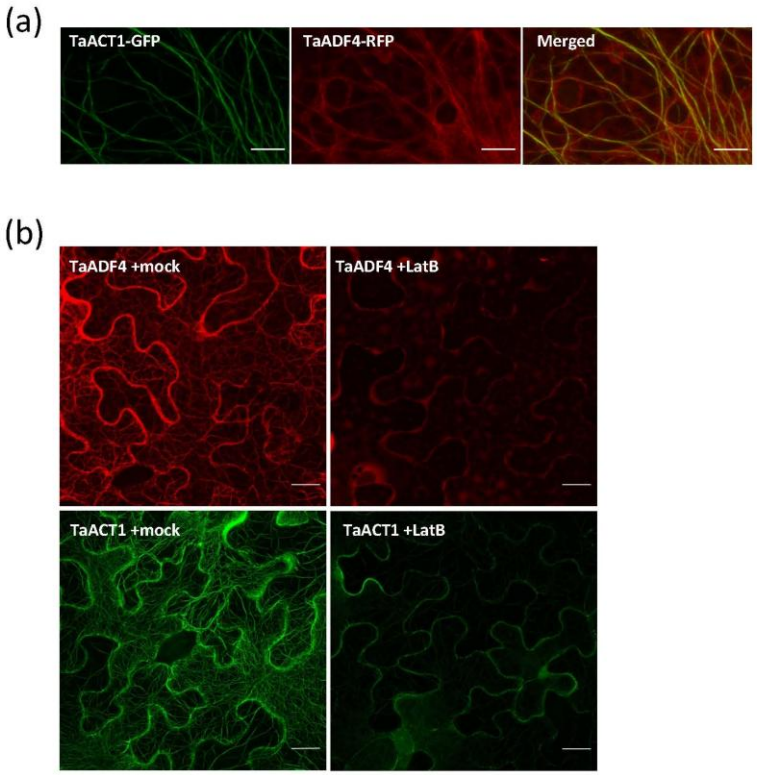

Figure 3. *Ta*ADF4 localizes to actin filaments.
(a) Images of transiently expressed *Ta*ACT1-GFP and *Ta*ADF4-RFP in *Nicotiana benthamiana* were taken by laser scanning confocal microscopy. Bar = 10 µm.
(b) LatB treatment of cells expressing *Ta*ADF4-RFP and *Ta*ACT1-GFP results in filament depolymerization and dissociation of *Ta*ADF4-RFP from F-actin structures. Bar = 10 µm.

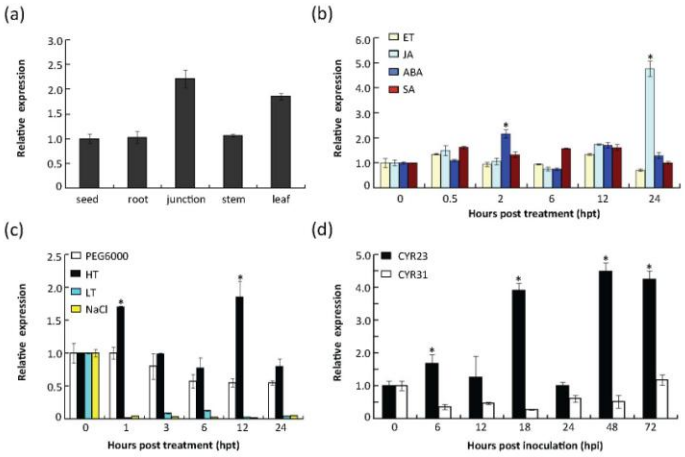

Figure 4. *TaADF4* mRNA accumulation is induced in response to hormone treatment, abiotic, and biotic stress perception.
(a) Real-time PCR analysis of *TaADF4* mRNA accumulation from various wheat tissue types.
(b) *Ta*ADF4 expression is induced following abscisic acid (ABA) and methyl-JA (JA) perception. qRT-PCR analysis of *TaADF4* mRNA accumulation in leaves of Suwon 11 following hormone treatment. Leaves were treated with, individually, ethylene (ET), methyl-JA, ABA, and salicylic acid (SA), and samples were collected at 0-24 hours post-treatment (hpt). * Indicates statistically significant difference between incompatible and compatible interactions ($P < 0.05$). All data were normalized using the internal control expression of *TaEF-1α*. Error bars represent the standard deviation of expression from three independent biological replicates.
(c) *TaADF4* is rapidly induced in response to high-temperature, and down-regulated in response to drought, low-temperature, and salinity. qRT-PCR analysis of *TaADF4* mRNA accumulation in response to abiotic stress perception. Suwon 11 leaves were stimulated with PEG6000 (drought simulation), high-temperature (HT), low-temperature (LT), and high salinity (NaCl), and mRNA expression was quantified at time intervals between 0 and 24 hpt. * Indicates statistically significant difference between incompatible and compatible interactions ($P < 0.05$). All data were normalized using the internal control expression of *TaEF-1α*. Error bars represent the standard deviation of expression from three independent biological replicates.
(d) *TaADF4* mRNA expression is rapidly induced in response to inoculation with the virulent *Pst* strain CYR23. qRT-PCR analysis of *TaADF4* mRNA accumulation in Suwon 11 leaves after inoculation with *Pst* CYR23 (incompatible) and *Pst* CYR31 (compatible). * Indicates statistically significant difference between incompatible and compatible interactions ($P < 0.05$). All data were normalized using the internal control expression of *TaEF-1α*. Error bars represent the standard deviation of expression from three independent biological replicates.

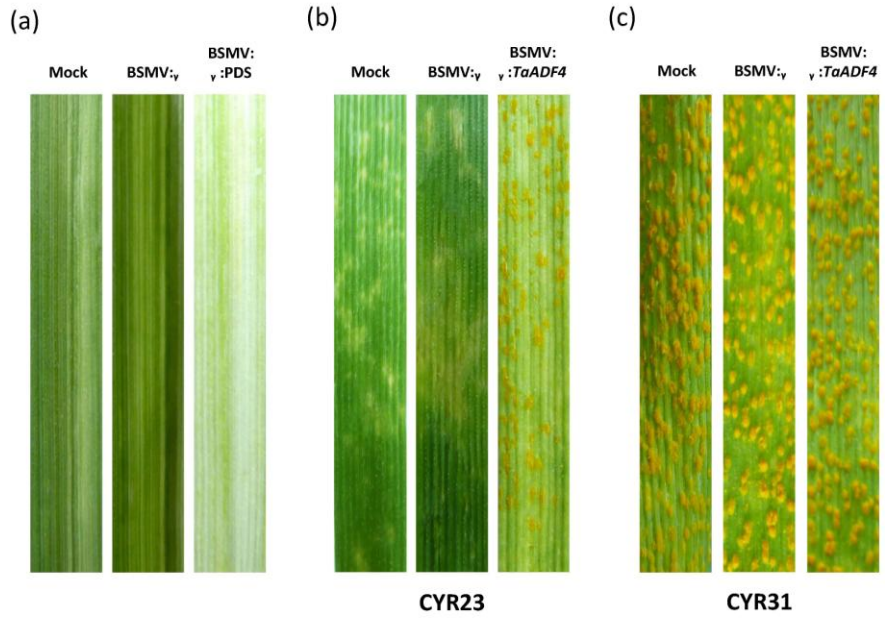

Figure 5. Silencing of *Ta*ADF4 in wheat renders plants susceptible to *Pst* CYR23.
Infection phenotypes of mock, BSMV:$_{\gamma}$, BSMV:$_{\gamma}$:PDS, and BSMV:$_{\gamma}$:*TaADF4* wheat leaves at 15 dpi.
(a) Control wheat lines, consisting of mock- (Fes buffer), BSMV:$_{\gamma}$-, and BSMV:$_{\gamma}$:PDS-transformed lines. No pathogen inoculation.
(b) Mock-, BSMV:$_{\gamma}$-, and BSMV:$_{\gamma}$:*TaADF4*-transformed lines inoculated with *Pst* CYR23.
(c) Mock-, BSMV:$_{\gamma}$-, and BSMV:$_{\gamma}$:*TaADF4*-transformed lines inoculated with *Pst* CYR31.

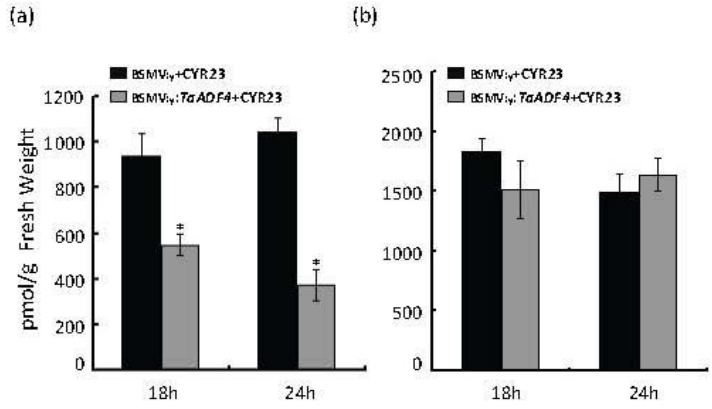

Figure 6. Jasmonic acid levels are reduced in *Pst* CYR23-inoculated *TaADF4* silenced plants.
(a) Jasmonic Acid (JA) levels after plants inoculated with *Pst* CYR23 at 18 and 24 hpi.
(b) Salicylic acid (SA) levels remain unchanged in *TaADF4* silenced plants following inoculation with *Pst* CYR23 at 18 and 24 hpi. Data shown is from three biological replicates. Error bars represent the standard deviation of expression from three independent biological replicates. * Indicates statistically significant differences in JA accumulation between WT and *TaADF4* RNAi-silenced plants ($P < 0.05$).

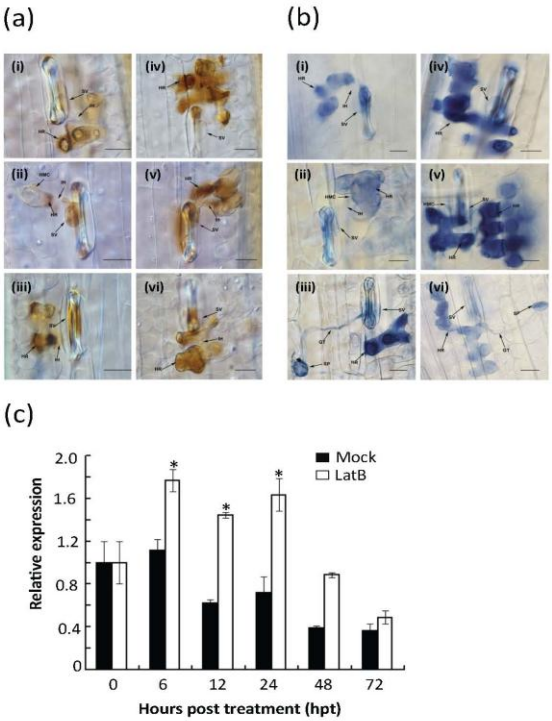

Figure 7. Treatment of wheat leaves with latrunculin-B enhances defense responses and abrogates *Pst* infection.
(a) Histological observation of H_2O_2 accumulation in mock treatment (i-iii) and LatB-treated (iv-vi) wheat leaves inoculated with *Pst* CYR23.
(b) Histological observation of hypersensitive cell death in wheat leaves inoculated with *Pst* CYR23. i-iii, mock. iv-vi, LatB treatment. Blue (trypan) staining indicates hypersensitive cell death. SP, spore; GT, germ tube; SV, sub-stomatal vesicle; HMC, haustorial mother cell; IH, infection hypha; HR, hypersensitive response. Bar = 25 μm.
(c) The expression level of *TaADF4* mRNA in Suwon 11 leaves following infiltration with LatB, and mock-inoculation. * Indicates statistically significant differences between treatments ($P < 0.05$). All data were normalized to *TaEF-1α* expression levels. Error bars represent the standard deviation of expression from three independent biological replicates.